Design and Fabrication of a Test Board Assembly for a Silicon Photonics LIDAR Device

Design and Fabrication of a Test Board Assembly for a Silicon Photonics LIDAR Device

Antonio Fincato[1], Daniele Caltabiano[1], Filippo Carastro[1], Luca Maggi[1], Mark Shaw[1], Paolo Diotti[1], Aina Serrano Rodrigo[2], Davide Rotta[2], Marco Chiesa[2], Linda Gianini[3,4], Matteo Galli[3], Daniele Bajoni[3]
STMicroelectronics Srl[1], Camgraphic srl[2], Università di Pavia[3], Univ. Grenoble Alpes & CEA-LETI[4]

Abstract

The development of Silicon Photonics LIDAR (Laser Imaging, Detection, And Ranging) devices for applications such as autonomous driving has been progressing with many different approaches that can be used to achieve the LIDAR transmitter device mostly based on an Optical Phased Array (OPA). In this paper two different approaches at the eye safe 1550nm range are described: - a Silicon Photonics LIDAR based on OPA's with a simplified electrical driving architecture and an array of Mach-Zehnder (MZ) interferometers, - an only MZ device used to switch the light output between grating devices to provide beam steering of the LIDAR beam. The design for a Test Board of a Silicon Photonics LIDAR device incorporating a control system for controlling the OPA and the matrix of MZ switches is outlined along with the LIDAR packaging, assembly, and the alignment of collimating lenses to enable the angular deflection of the LIDAR device.

Introduction

In a Silicon Photonics LIDAR based on OPA devices [1,2,3] the input beam is split and the phase in each split branch controlled and altered so that when the final beams reach the output optical gratings and are emitted, the interference of the beams from the multiple branches will cause interference between the individual beams altering the wave front angle. The phase alteration design can be based on different architectures and the phase change devices based on TPM (Thermal Phase Shifters) or p-i-n junction PM (Phase Modulators) etc. To correctly control the phase, each individual Phase Shifter has to be controlled in order that a smooth variation of the wavefront is obtained.

An alternative method to obtain the variation of beam direction is to directly switch the output signal between the optical gratings, this combined with a suitable optical system that collimates and angles differently the beams from each individual grating performs the necessary beam steering.

Silicon Photonics OPA LIDAR design

In Fig. 1, OPA LIDAR design [1] [2] is based on 1x32 OPA utilising thermal phase shifters to modify the phase of the light in each split branch, once recombined at the optical grating, this guarantees a beam steering of about 2 degrees. This angle can be increased by modifying the design (pitch and dimensions of the individual grating) and increasing the number of elements in the OPA, as the resolution is limited by reduced number of elements in OPA (32). However, combining different OPA's, it is possible to obtain a wider scanning angle limiting the overall energy consumption of the phase shifters. Each OPA is designed, with an optical delay circuit in respect to the other OPA's, realized with an array of waveguides with linear increasing length which introduces a linearly increasing phase offset. This phase offset generates on the output beam a fixed interference causing a bending angle respectively of -3°, -1°, 1° and 3°. A switching matrix, 1x4 selects each block of OPA's in a consecutive way between the OPA's with different fixed phase offsets, and the beam steering is done sequentially around the fixed offset.

In this way, the total scanning angle covers 4 times the range of a single OPA without increasing the electrical power consumption of the phase shifter network, except for the power dissipated in the switch matrix, that is much smaller than that dissipated inside each OPA. As a result, total scanning angle of about 8 degrees is obtained.

Sketches of OPA and switching matrix are depicted in Fig. 1 and Fig. 2 respectively, while the complete TX is shown in Fig.3

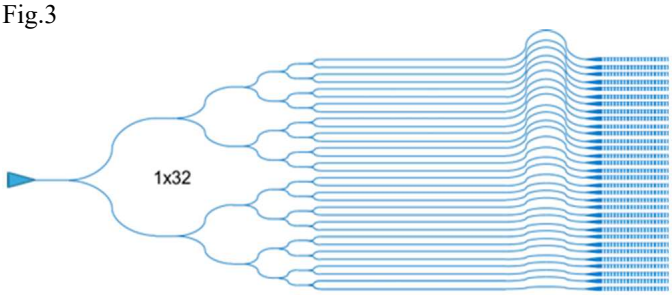

Fig. 1. OPA 1 x 32

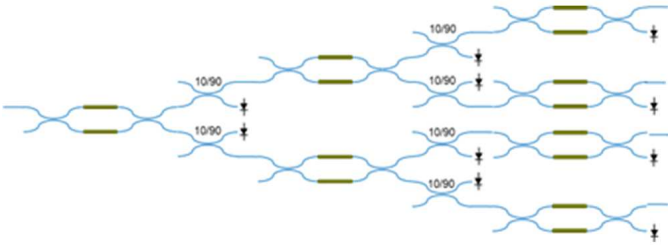

Fig. 2. Switching matrix 1 x 4

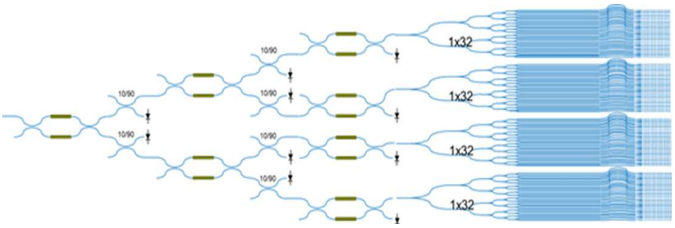

Fig. 3. complete TX., angular offset is clearly visible before each OPA.

The basic cell of switching matrix is a Mach-Zehnder interferometer modulator followed by a directional coupler tap and a monitor photodetector, and a PIN-PM acting as Variable Optical Attenuator (VOA) to guarantee the proper signal suppression and equalization. This basic cell (Fig.5) is characterised by the following key parameters: Extinction Ratio (ER) = 23 dB, Insertion Loss (IL) = 1.1 dB.

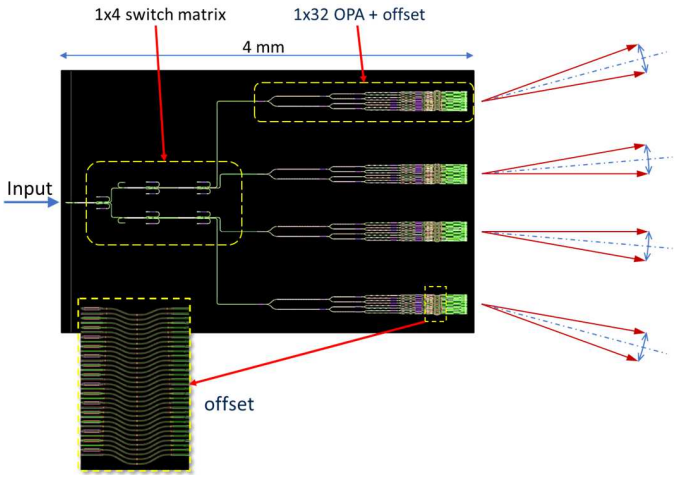

Fig. 4. Working principle of MZ OPA

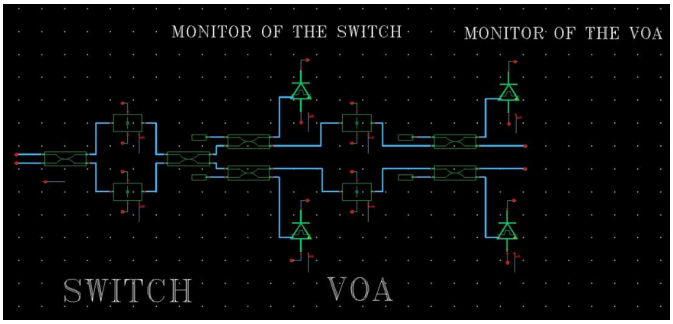

Fig. 5. basic cell of switching matrix

Inside each OPA, Thermal Phase Shifter (TPS) is used for generating the proper phase difference between each emitting grating, for addressing the desired beam steering. There is a series of TPS for adding and a second series for subtracting the phase difference, and GND is common to all TPS.

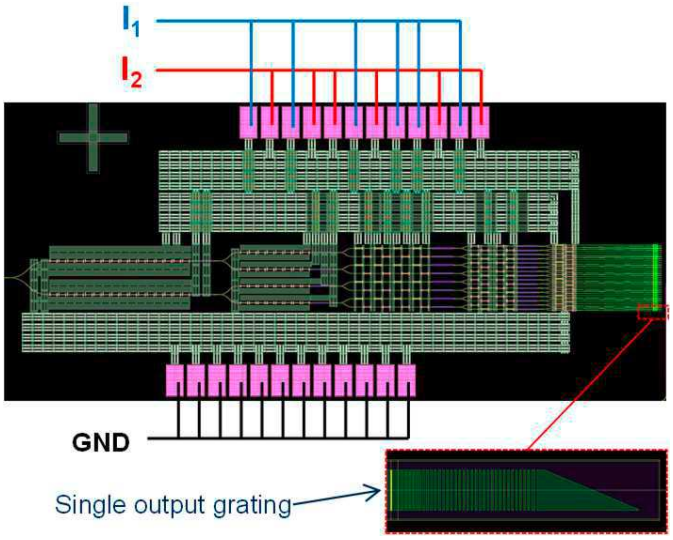

Fig. 6. Electrical connections to TPS

In this architecture the electrical control is shared for all the phase shifters with an architecture requiring two driving electrical signals only (plus ground) for N optical antennas, whichever is the value of N. The drive circuit for the OPA is therefore much simplified, when a current I1 (I2) feeds the first (second) network of thermal phase shifters, a phase delay is generated, and the output beam is positively (by I1) or negatively (by I2) angularly deflected. (fig.6).

So, for the four OPAs of complete transmitter, eight different signals are required, but only one at a time is used. In Addition to these, the switch matrix requires 8 signals for each MZ, 24 plus ground in total.

Silicon Photonics MZ switch Lidar Design

If we take the idea of using the MZ approach further and construct a Lidar device based only on the MZ switches this can be done by switching from one grating to another in the array and combining it with an optical system such that each emitted beam is inclined at a certain angle with respect to the adjacent ones. In this way as the light is switched between the gratings the angle of the beam is changed.

In this paper we are describing an array of 64 (4x16) Grating Couplers (GC). Each GC in the array is fed by a switching matrix based on cascaded Mach Zehnder interferometers. To obtain the proper signal equalization, each branch of last stage MZ is monitored, so at the end there are 64 monitor circuits (32 MZ*2 branches/MZ).

The working scheme of the optical circuit is shown in Fig. 7, and the physical layout is represented in Fig. 8

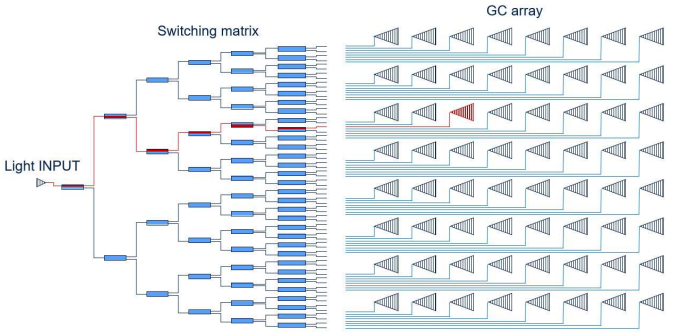

Fig. 7. schematic of MZ switch LIDAR

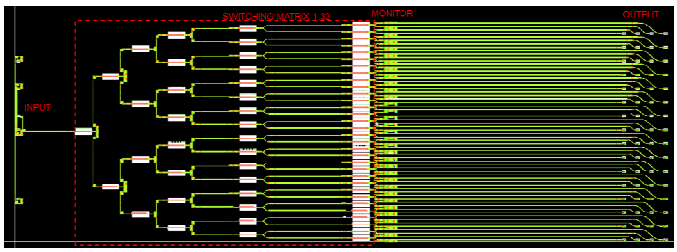

Fig. 8. chip Layout of MZ switch LIDAR

To keep a manageable number of electrical I/O's, all MZ's, in every stage of the switching matrix, have common electrode for 0 V and 2V and all Photo Detectors (PD) have common anode. Each MZ has its own electrode varying from 0 to 2 V and each PD has its own cathode. The Working principle of electrical circuit is shown in Fig. 9

The pads for wire bonding are placed in North and South sides of the chip. West side can accommodate a fibre block for light insertion, while the East side is reserved for the placement of the lens array. To simplifying the coarse alignment, some metal markers are placed on top of the chip.

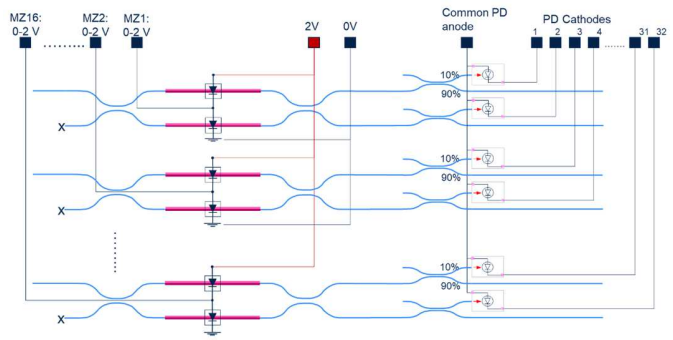

Fig. 9. schematic of MZ electrical circuit

The MZs are designed in "through mode", so that when they are not connected or switched off, most of the light travels over the upper output and a nearly negligible fraction through the lower output (Fig. 9). This configuration is useful during assembly since it is possible to proceed without electrically connecting the device. It can also be useful during testing as a single output will be obtained with each stage of the MZ switches.

Packaging

To test the OPA based design concept a chip with only the 1x32+offset OPA section has been assembled. In the prototype Packaging an external light source is used, and the optical signal is delivered by an optical fibre fixed through an angled polished V-groove aligned and glued with UV curable epoxy to the input optical grating. Good alignment and low losses are obtained by using additional gratings external to the signal grating which are connected internally to the LIDAR chip so the optical loss of the alignment loop can be measured and optimised during the alignment. This process is outlined in more detail in the section on the MZ device (4). The fibre array overlapped the edge of the OPA device so the die was diced to a large size including other die on the Multi product wafer (Fig. 10), this ensures that during the UV curing any post cure movement is minimised and that that there is no excess epoxy at the chip edge.

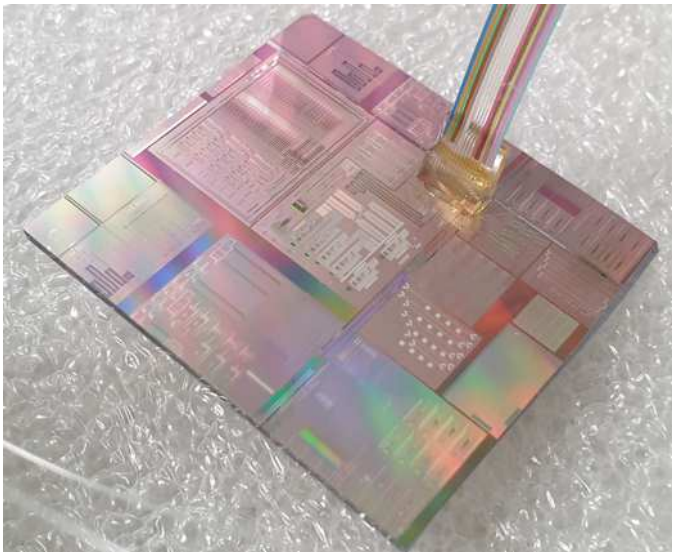
Fig. 10. fibre attached to OPA

Since the electrical drive system is extremely simplified and can be driven with a limited number of electrical connections, no additional prototype packaging was performed as the device can be driven with the use of only 3 external optical probes for the 1x32 OPA. In a final prototype the packaging will be similar to that outlined in the following section for the MZ device.

The packaging of the MZ switch Lidar is more complicated as each individual MZ's must be controlled and connected to the package. A two-stage packaging approach has been utilized: the MZ LIDAR device is first packaged onto a daughter board, and then mounted on a control mother board (Fig. 11). The photocurrents of the Photodiodes are used as feedback for controlling the MZ in the switch matrix.

The control circuit must drive each individual MZ switch to allow optical output power to be switched between gratings. To ensure a uniform temperature across the devices, the die is assembled on a copper heatsink inserted into a cavity within the daughterboard PCB using conductive epoxy (5). In this way, when the MZ switches are operating, there are no relative changes in optical path length due to temperature. The height of the cavity is designed so that the die protrudes from the substrate PCB by approx. 0.1mm, this is to allow the optical vision system to view the edge of the chip and check parallelism with the optical fibre array and lens array during alignment.

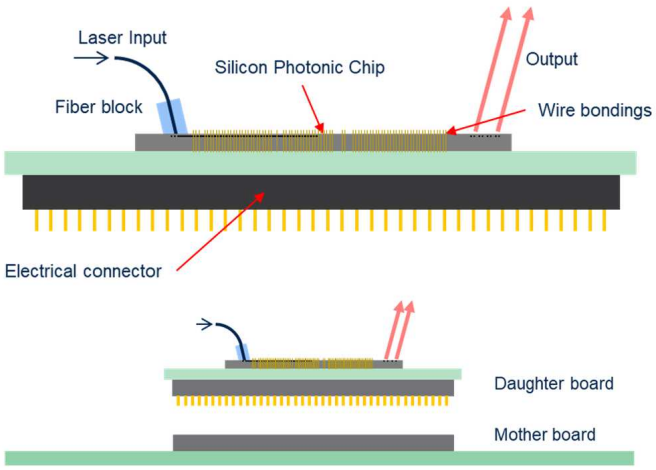

Fig. 11. Schematic of daughter board with mother board

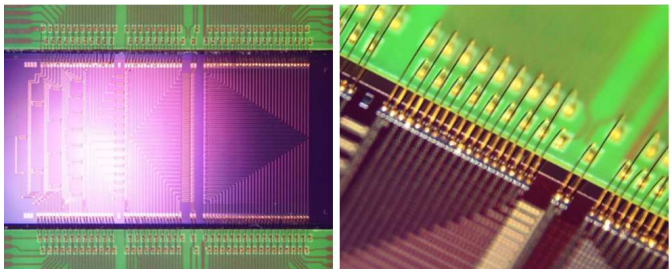
Fig. 12. Assembled die and wirebonding detail

A standard fibre array has been coupled into the input grating couplers of the PIC via a standard pigtailing procedure consisting of: (i) Fibre array passive positioning over the input grating couplers (Fig 13). This is possible due to the dedicated alignment markers in the chip and a pattern recognition image processing aid with the visible top camera. Angular control is

obtained via the image of the fibre array and die via the image from 45 degree mirrors in the top camera (ii) Active alignment. The fibre array position and angles are actively optimized by means of a peak picking procedure to minimize insertion losses of the alignment loop within\ between two fibres as wide apart as possible on the array, two input gratings and the optical loop within the die. (iii) Epoxy dispensing and curing. The fibre array is then fixed to the device with an index matching UV curable epoxy (Fig 14).

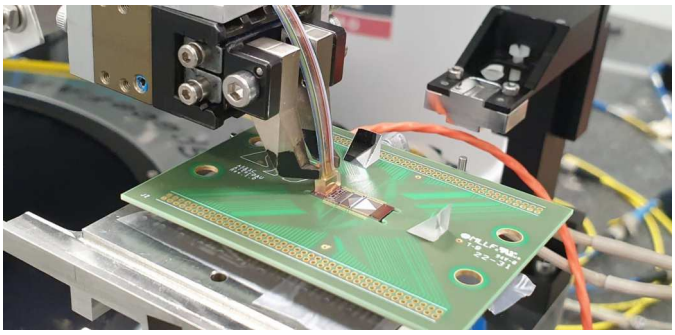

Fig. 13. alignment of fibre assembly on MZ Die

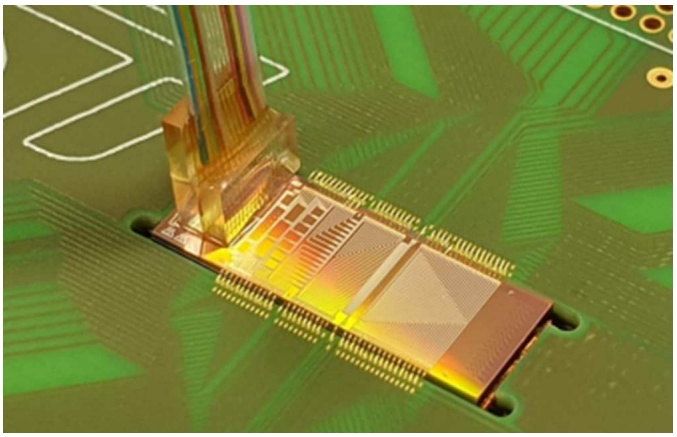

Fig. 14. assembled fire on MZ assembly

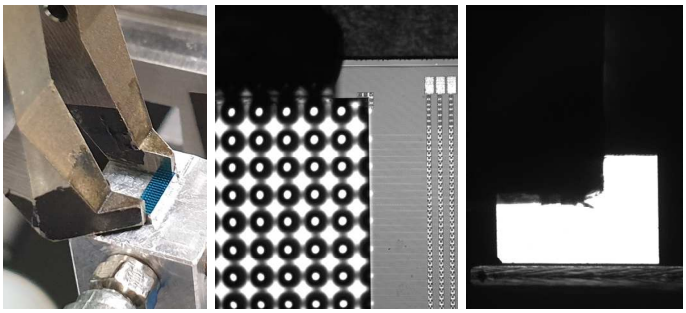

Fig. 15. Lens array preliminary passive alignment. a) Micro lens array pick up with alignment bench. b) Top and c) profile view of the lens array and chip during passive alignment

In these conditions, the centre of the IR camera corresponds to the emitting point of the grating couplers. Optimizing the lens array position in the plane and focusing distance (distance between lens array and PIC surface), the intensity and position of the obtained spot can be maximized. The alignment is done without electrically connecting the device as previously explained the devices switched off one grating is always illuminated even with the device electrically not connected.

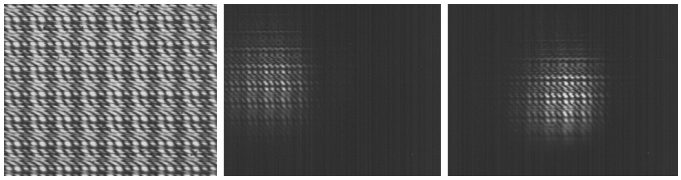

Fig. 16. IR camera images of Far field grating array during lens array alignment. a) Initial image without lens array; b) After first passive positioning of the collimating lens array; c) Final far field grating array image after lens array position optimization.

The coupling of the lens array to the PIC consisted in a first passive alignment over the output grating couplers, following a similar procedure used for fibre array (Fig. 15). An active alignment process has been performed to optimize the position of the lens array and ensure the collimation of the PIC output beams. To this end, an external laser has been coupled to the PIC through the previously pigtailed fibre array.

The IR camera, which position has been previously calibrated, has been placed orthogonally to the chip surface at a distance of 20cm. Fig. 16 shows the obtained IR camera images during the lens array alignment procedure. Specifically, Fig. 16-a shows the resulting far field interference pattern of the outcoming light from the output grating matrix without the collimating lens array. After the passive placement of the lens array in x and y by using the edges of the array to the alignment marks on the silicon photonics die, a misaligned spot image is obtained (Fig. 16-b). After the active optimization of the lens array position, the spot is more intense and aligned to the centre of the camera Fig. 16-c. After the complete alignment procedure in air, thermal optical epoxy has been dispensed to fix the lens array to the PIC. Due to the difference in refractive index between air and epoxy, minimum corrections in the lens array position are performed. Finally, thermal curing of the epoxy has been performed on the alignment bench. A glob top coating is added to protect the wirebonds form handling damage to complete the packaged device (Fig 17).

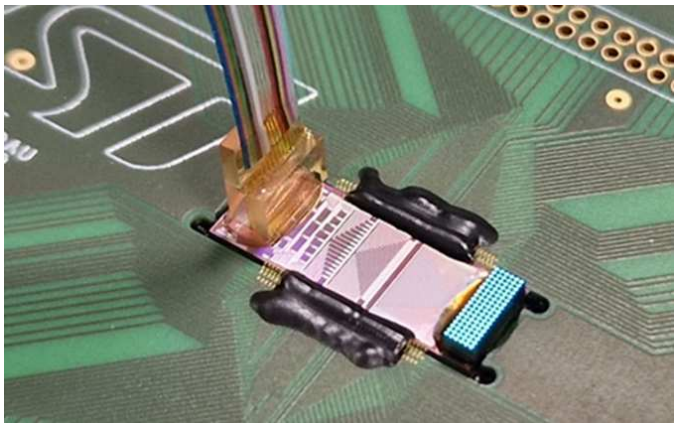

Fig. 17. Fully assembled daughter board with aligned microlenses

MZ LIDAR control mother board design

The control mother board for the MZ Lidar, shown in the schematic (Fig 18), consist of: 1) 64 Transimpedance Amplifiers (TIA), to amplify the PDs signals before the analogue to digital converter inputs of the microcontrollers 2) 4 STM32 microcontrollers, which receive the PD readings and compute the correct voltage values to be applied to the MZ tree; 3) six buffers (BUF), used to amplify the microcontroller outputs and provide enough current for the MZ switches; 4) a Multiplexer stage (MUX), which takes the amplified outputs from the buffers and set the proper MZ voltages;

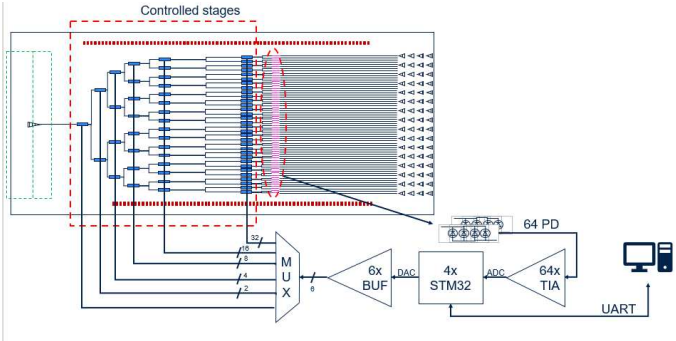

Fig. 18. control board schematic

When controlled correctly, six cascaded MZs only are required to select a specific output grating from the 64. The 6 MZ's to be controlled are selected via the microcontroller by exploiting the MUX block.

In this first version of the system only the first 4 stages are controlled, instead of the full network, corresponding to the 16 rows of the output gratings; the sum of 4 monitor photocurrents of each row is considered as a "Macro pixel", and used to verify the operation of the control loop. Since all the MZs have an approximately 90/10 splitting ratio when not controlled, the output power in the 4 gratings of each row have a relative distribution so that even when the final stages are not controlled the light is mainly emitted by only one grating. Therefore, in this first implementation, only 16 TIAs, one STM32 and 4 buffers are used.

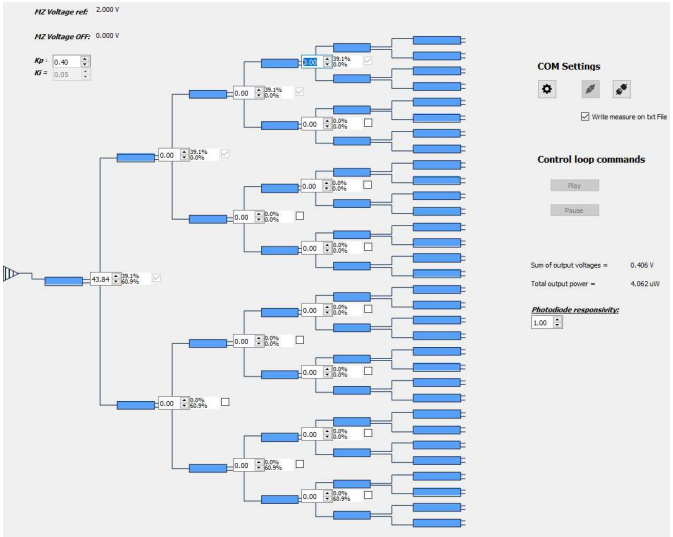

Fig. 19. Graphical User Interface

The Graphical User Interface (GUI), shown in Fig. 19 is used to monitor the status of the switch matrix in real time and allows the selection, via checker-boxes, of the output pixel.

In particular, the microcontroller sends the PDs readings to the GUI. The GUI computes and displays the normalized percentage of light for each MZ stage.

In the same way, when the user selects a different output pixel on the GUI via the checker-boxes, a message is sent to the microcontroller which than apply the new configuration to the output MUX in order to drive the proper MZ for each stage.

In this Lidar control system, a Perturb and Observe (P&O) control is used to find the Maximum Power Point (MPP) of each Mach-Zehnder output. This control system operates by perturbing the input voltage of the Mach-Zehnder interferometer and observing the resulting change in the output power from monitor photodiodes (fig 20). The algorithm then adjusts the input voltage in the direction of the observed change until the power output reaches its maximum value.

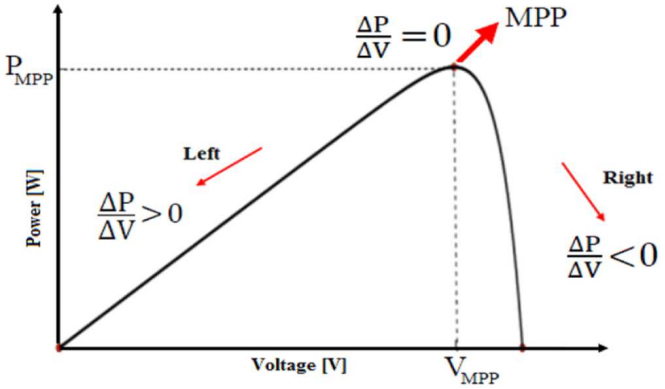

Fig. 20. Power vs Voltage for MPP

The first four stages of the switch matrix of Fig. 18, that is the first 1x16 switch tree, have been controlled with the algorithm described above, and the results, as read from the graphical interface of Fig. 19, is summarized in Fig. 21. In this graph the percentage of all the power transmitted inside the matrix and driven in each of the 16 output rows, is reported.

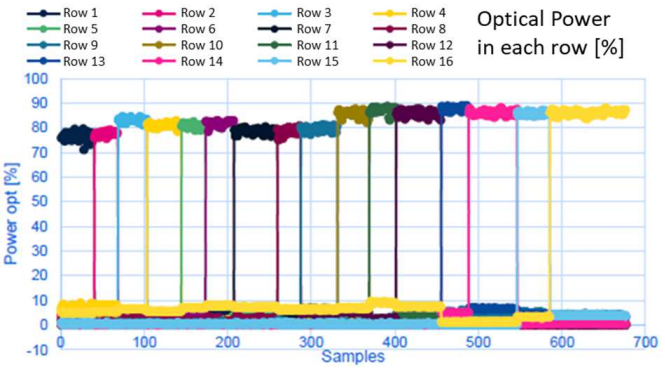

Fig. 21. PD current using 4 MZ stages

OPA LIDAR Measurements

The OPAs shown in Fig. 6 have been realized in a separate chip without the switch matrix, with the intention of

independently characterize them. They were first characterized in Far Field condition, and the comparison between measurements and simulation is shown in Fig. 22. It is possible to see the zero-order interference fringe and the weaker interference fringes of order 1 at +/-9°.

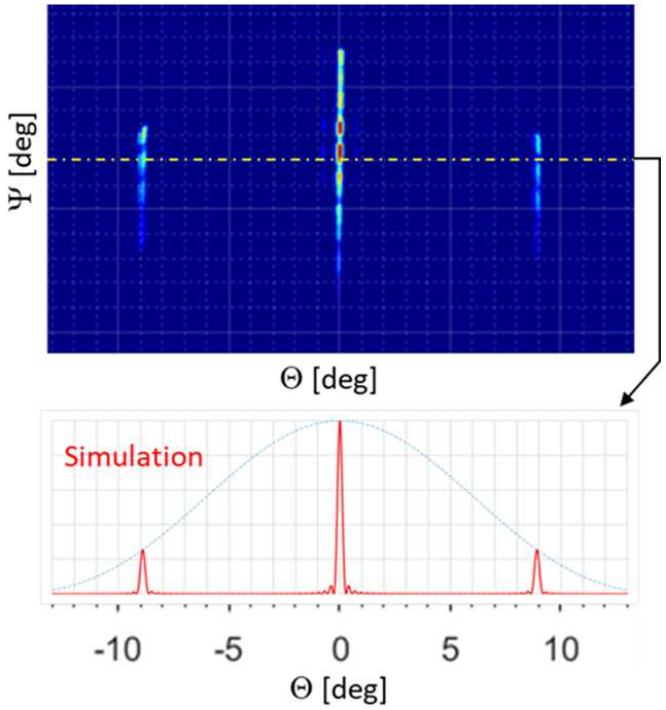

Fig. 22. grating output simulation vs actual

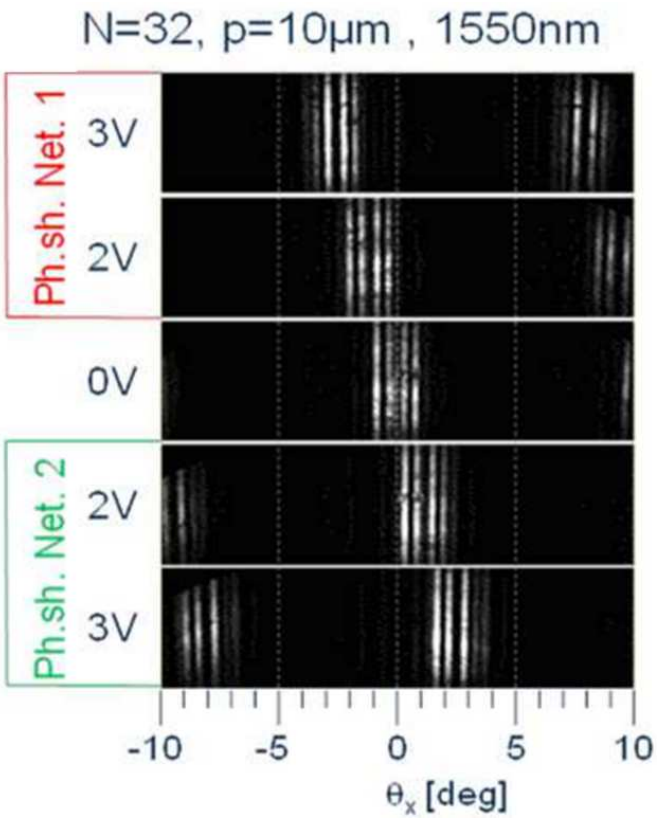

Fig. 23. Beam steering of optical output.

With two electrical signals applied sequentially to the two phase shifter networks, it is possible to obtain a beam steering angle in the range θx =±2.5deg (fig. 23) linearly proportional to the electrical power dissipated into the phase shifter network (fig. 24) at a rate of 1.5deg/W. The relatively high value of the dissipated electrical power, it is due to a non optimised thermal phase shifter used in this device, that has a Pπ≈40mW.

The polar angle θy can be controlled with a tunable laser by sweeping the wavelength at a rate of 0.1°/nm (fig. 25) with a linear dependence for at least 80nm, also in this case the low rate value is due to the grating coupler that it is not optimized for this application.

Weaker side lobes of the beam appear when a voltage is applied due to the random phase errors occurring along the 3.5mm long device.

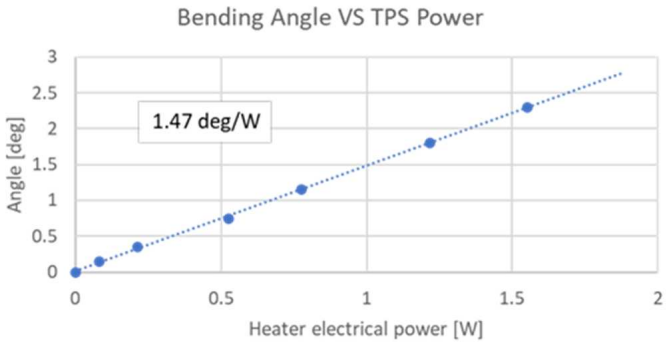

Fig. 24. beam steering angle vs power consumption

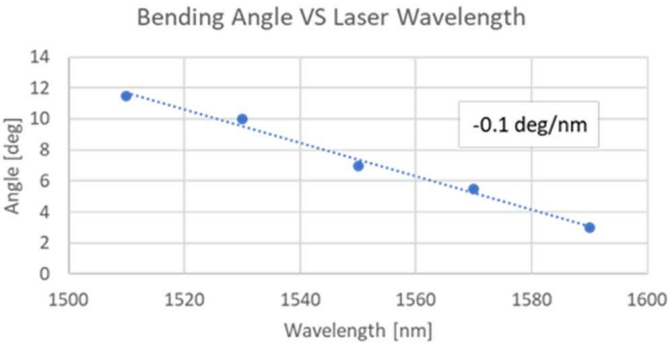

Fig. 25. beam steering angle vs laser wavelength

MZ switch LIDAR results.

Fig. 26 shows the test set up for Far Field characterization of the MZ-switch LIDAR, with an IR camera placed at 50mm from the chip surface. The chip is assembled on the daughter board plugged into the control mother board. Using the graphical interface, the light is switched in the MZ matrix between the output gratings to produce a swept collimated beam suitable for LIDAR devices. The camera has no mounted objectives but only a neutral filter to reduce the power collected by the CCD sensors.

In Fig 27a three superimposed images show the light output beam switched using only the first three stages of the matrix. In this case eight different gratings (two rows) are illuminated, but since the not-controlled MZ in the later stages have a splitting ratio of 90/10 (as previously stated), the light is still channelled predominantly through a single grating. However, the movement of the spot between the gratings (red

arrow) is clearly seen as switching is performed between the different rows of gratings. In one case only it is possible to select one single grating among the 64, and in Fig. 27b it is possible to observe the single spot formed from this grating with its microlenses when all 6 MZ stages are controlled.

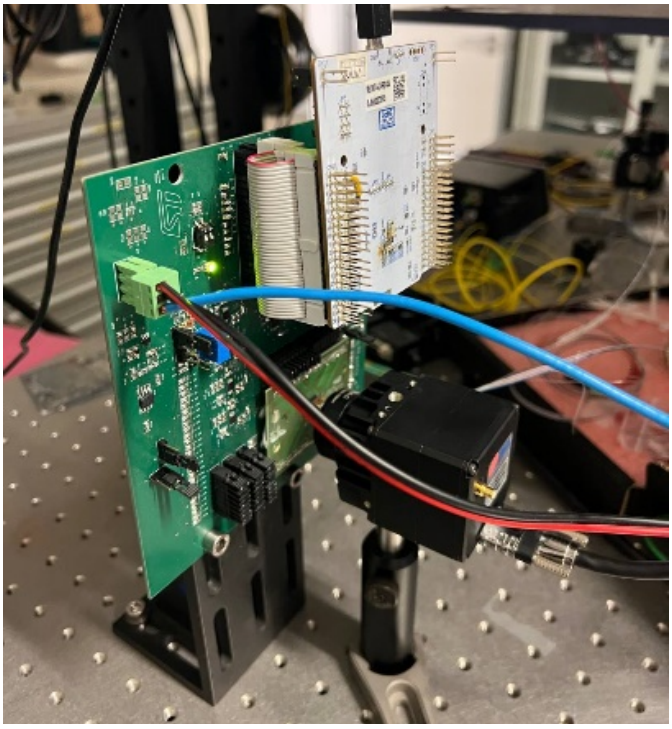

Fig. 26. test set up

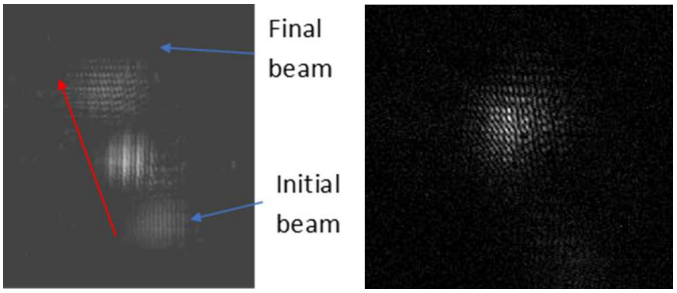

Fig. 27. a) collimated beam position movement using 3 MZ stages b) single spot with all MZ stages controlled

Optical System for MZ Beam Steering.

Above the switching of the output beam has been demonstrated between the Output gratings but with only a lens system on a standard pitch this produces only the stitching between collimate beams and no beam steering. To produce beam steering an optical system is required that modifies the angle of the collimated beam for each beam. This can be done by using an array of micro-prisms with the same pitch of the microlenses and realized with different angles to deflect the collimated beams emerging from the microlenses in different directions. In this way it is possible to cover a wide Field-of-view selecting sequentially with the switch matrix all the output gratings.

Conclusion

2 different architectures for the inclusion of MZ structures within a LIDAR system have been outlined along with the necessary control system and packaging, demonstrating the feasibility of each of the LIDAR structures. The structure with the combined MZ and OPA system shows the effectiveness of a simplified control system, however the current TPS phase shifter has a high current consumption. The MZ switch device shows a possible architecture for a much reduced current consumption but it requires integration with a more complicated optical system. Any device will need to be scaled up with tens of thousands of gratings, increasing the overall power consumption, however the development of LIDAR systems based on silicon photonics shows promise for the requirements of autonomous driving, reduced power consumption is required and alternative phase change device elements are need and the use of these along with MZ in different architectures could produce viable low power consumption devices.

Further Work

Further work would include full characterisation of the MZ switch based LIDAR transmitter along with the design fabrication and assembly of the optical system necessary for the beam steering along with the assembly and testing of the combined MZ-OPA device.

References

1. M. Zadka, Y. Chang, A. Mohanty, C. Phare, S. Roberts, and M. Lipson, "On-chip platform for a phased array with minimal beam divergence and wide field-of-view," Opt. Express 26, 2528-2534 (2018).
2 T. Kim et al., "A Single-Chip Optical Phased Array in a Wafer-Scale Silicon Photonics/CMOS 3D-Integration Platform," in IEEE Journal of Solid-State Circuits, vol. 54, no. 11, pp. 3061-3074, Nov. 2019
3 S. Ura, J. Inoue and K. Kintaka, "Vertically Stacked and Directionally Coupled Cavity-Resonator-Integrated Grating Couplers for Integrated-Optic Beam Steering," 2019 IEEE 69th Electronic Components and Technology Conference (ECTC), Las Vegas, NV, USA, 2019, pp. 556-562.
4 A. Bazzotti, M. Fere, L. Maggi and M. Shaw, "Silicon photonics assembly industrialisation," 2015 European Microelectronics Packaging Conference (EMPC), Friedrichshafen, Germany, 2015, pp. 1-6.
5 M. Binda et al., "High Capacity Silicon Photonics Packaging," 2019 22nd European Microelectronics and Packaging Conference & Exhibition (EMPC), Pisa, Italy, 2019, pp. 1-8.